

Theoretical Estimates of Light Reflection and Transmission by Spatially Complex and Temporally Varying Sea Ice Covers

DONALD K. PEROVICH

U.S. Army Cold Regions Research and Engineering Laboratory, Hanover, New Hampshire

The reflection, absorption, and transmission of light at visible and near-infrared wavelengths by snow and ice covers is important for a number of geophysical problems. The focus of this paper is on the reflection and transmission of light by spatially inhomogeneous and temporally varying sea ice covers. This is investigated using a two-stream, multilayer radiative transfer model in the wavelength region from 400 to 1000 nm. The model is computationally simple and utilizes the available experimental data on the optical properties of sea ice. The ice cover is characterized as a layered medium composed of selections from nine distinct snow and ice types. Three case studies are presented illustrating values of spectral albedo, transmittance, and transmitted photosynthetically active radiation (PAR) for (1) a spatially inhomogeneous ice cover, (2) a uniform ice cover as it undergoes a melt cycle, and (3) a temporally changing spatially variable ice cover. Results indicate that small-scale horizontal variations in snow depth and ice thickness can cause light transmission to change over 3 orders of magnitude. Dramatic changes in light reflection and transmission are predicted in the early part of the melt season as the ice cover evolves from an opaque, snow-covered medium to translucent bare or ponded ice.

INTRODUCTION

The reflection, absorption, and transmission of shortwave radiation by a sea ice cover is significant in a variety of geophysical problems. Spectral reflectance is important in the interpretation of imagery from remote sensing instruments operating at visible and near-infrared wavelengths. *Maykut and Untersteiner* [1971], *Grenfell and Maykut* [1977], and *Maykut and Perovich* [1987] have established the critical role played by shortwave radiation in the heat balance of a sea ice cover. Primary productivity and other biological activity under the ice are strongly affected by amount and spectral composition of transmitted light [*SooHoo et al.*, 1987].

Because of this established importance there is a substantial data base of optical measurements of reflected and transmitted light for sea ice. Observational data on the optical properties of sea ice and of snow are reviewed by *Perovich et al.*, [1986] and *Warren* [1982], respectively. These observations indicate that understanding radiative transfer in ice and snow is considerably complicated by the large temporal and spatial variability in the physical, and therefore optical, properties of the medium. For example, observations indicate that as a snow cover ages and metamorphism increases its grain size, there is a decrease in albedo [*Grenfell and Perovich*, 1981]. The physical structure of sea ice can be even more complex, with vertical variations in vapor inclusions, ice temperature, salinity, and brine volume. Observations have demonstrated that the optical properties of sea ice depend on the ice temperature, brine volume [*Perovich and Grenfell*, 1981; *Buckley and Trodahl*, 1987], and surface conditions [*Grenfell and Maykut*, 1977].

This complexity necessitates use of theoretical models both to interpret and to extrapolate the observational data. Over the years, several different models have been formulated to describe radiative transfer in sea ice. *Dunkle and*

Bevans [1956] formulated a model, based on the work of *Schuster* [1905], to calculate the upwelling and downwelling irradiance in a snowpack. This model was used by *Grenfell and Maykut* [1977], *Grenfell* [1979], and *Perovich and Grenfell* [1981] to interpret field and laboratory measurements of the optical properties of sea ice. *Perovich and Grenfell* [1982], using the discrete ordinates method of *Chandrasekhar* [1960], developed a four-stream model to investigate the optical properties of young ice. *Grenfell* [1983] formulated a comprehensive 16-stream radiative transfer model for sea ice. His model not only provided a detailed description of the radiance field but also rigorously defined scattering in terms of the physical structure of the ice. *Trodahl et al.*, [1987] used a diffusive Monte Carlo model to investigate the angular and spatial distribution of the radiance transmitted and reflected by a sea ice cover.

These models all have features that both recommend and limit them for particular applications. Often there are trade-offs between detailed physics and computational simplicity. In this report we will develop and present a two-stream, multilayer model of radiative transfer at visible and near-infrared wavelengths. The two streams refer to the upwelling and downwelling irradiance. While this discussion is directed specifically toward a sea ice cover, the formulation is sufficiently general to be easily adapted to other translucent media such as lake ice, river ice, or turbid water. The major limitation of this model lies in its casual treatment of the physics of scattering, in particular in its assumption of isotropic scattering and the lack of information concerning the angular distribution of the radiation field. However, since our interest is in irradiance, the radiance integrated over angle, this is not a major difficulty. The model is also limited in its treatment of the effects of solar zenith angle on albedo. This is not a major difficulty because during the summer low stratus clouds are typically present over the sea ice, giving diffuse incident conditions.

The model has three primary advantages. Computationally, it is simple and fast, avoiding the numerical difficulties of more advanced methods such as 16-stream models. Thus

This paper is not subject to U.S. copyright. Published in 1990 by the American Geophysical Union.

it can be run quickly on a personal computer, allowing a wide range of cases to be investigated easily. In addition, this two-stream model can directly exploit the large observational data base of sea ice optical properties compiled by Grenfell and Maykut [1977], Grenfell [1979], and Perovich and Grenfell [1981]. Finally, only a qualitative depiction of the ice structure (blue ice, white ice, melting ice) is needed, rather than the detailed statistical description of the scattering inhomogeneities demanded by more sophisticated models.

THEORY

The model is two stream in that it calculates a downwelling (F_{\downarrow}) and an upwelling (F_{\uparrow}) irradiance in the medium. The irradiance is defined as the total energy per unit area per unit time (in watts per square meter incident on a horizontal plane from the lower (F_{\uparrow}) and upper (F_{\downarrow}) hemisphere. In the medium each layer is considered to be plane parallel, i.e., homogeneous in x , y , and z and infinite in extent in x and y . The optical properties of a layer are defined in terms of wavelength dependent scattering (r_{λ}) and extinction (κ_{λ}) coefficients. The downwelling and upwelling irradiances are governed by the coupled first-order differential equations

$$dF_{\downarrow}(z, \lambda) = -k_{\lambda}F_{\downarrow}(z, \lambda) dz - r_{\lambda}F_{\downarrow}(z, \lambda) dz + r_{\lambda}F_{\uparrow}(z, \lambda) dz \quad (1)$$

where the left-hand side is the change in downwelling and the terms on the right-hand side are loss to absorption, scattering loss from downwelling, and scattering gain from upwelling, and

$$dF_{\uparrow}(z, \lambda) = k_{\lambda}F_{\uparrow}(z, \lambda) dz - r_{\lambda}F_{\downarrow}(z, \lambda) dz + r_{\lambda}F_{\uparrow}(z, \lambda) dz \quad (2)$$

where the left-hand side is the change in upwelling and the terms on the right-hand side are loss to absorption, scattering gain from downwelling, and scattering loss from upwelling; z is the depth within the medium (increasing downward), and λ is the wavelength of the light. Scattering (r_{λ}) and absorption (k_{λ}) are treated through wavelength dependent coefficients. Together, the scattering and absorption coefficients define the extinction coefficient κ_{λ} , where $\kappa_{\lambda} = (k_{\lambda}^2 + 2k_{\lambda}r_{\lambda})^{0.5}$. If there is no scattering, (1) reduces to

$$dF_{\downarrow}(z, \lambda) = -k_{\lambda}F_{\downarrow}(z, \lambda) dz \quad (3)$$

which when integrated yields the familiar Bouguer-Lambert law

$$F_{\downarrow}(z, \lambda) \propto e^{-k_{\lambda}z}$$

Equation (2) reduces to $F_{\uparrow}(z, \lambda) = 0$ for the no scattering case. Equations (1) and (2) can be reformulated as uncoupled second-order differential equations [Perovich, 1989] with general solutions of

$$F_{\downarrow}(z, \lambda) = A \sinh(\kappa_{\lambda}z) + B \cosh(\kappa_{\lambda}z) \quad (4)$$

$$F_{\uparrow}(z, \lambda) = C \sinh(\kappa_{\lambda}z) + D \cosh(\kappa_{\lambda}z) \quad (5)$$

This method converges to a simple exponential decay for optically thick media, but as Grenfell [1979] points out, it

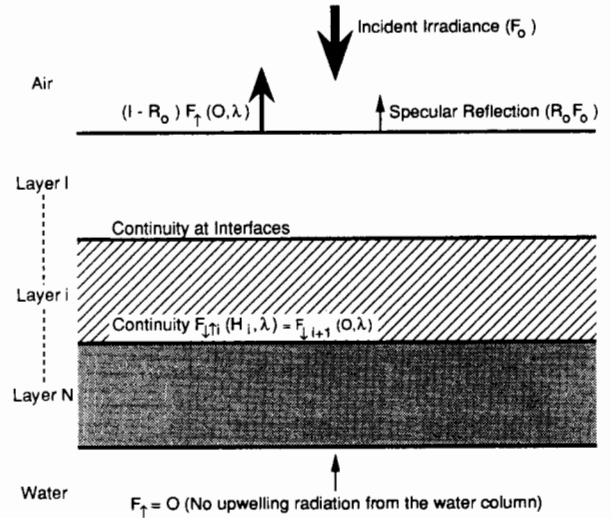


Fig. 1. Schematic of two-stream, N -layer model.

offers substantial improvements in accuracy over exponential decay for optically thin cases.

The geometry of the multilayer model is schematically illustrated in Figure 1. We consider N layers, with each layer i having thickness H_i and optical properties defined by the constants $\kappa_{\lambda i}$ and $r_{\lambda i}$. We assume that there is no specular reflection at the interfaces between layers. To specify the solution to (4) and (5) for a layer, it is necessary to determine the four constants A , B , C , and D . Hence $4N$ equations are needed to solve an N -layer system.

Two equations are provided by the surface and bottom boundary conditions. At the surface we have

$$F_{\downarrow 1}(0, \lambda) = (1 - R_0)F_0 + R_0 F_{\uparrow 1}(0, \lambda) \quad (6)$$

where F_0 is the incident solar irradiance and R_0 is the specular reflection at the surface. At the bottom boundary we assume that there is no specular reflection and there is no upwelling from below, yielding a boundary condition of

$$F_{\uparrow N}(H_N, \lambda) = 0 \quad (7)$$

We require continuity at the interfaces between layers. These matching conditions provide $2(N-1)$ equations of the form

$$F_{\downarrow i}(H_i, \lambda) = F_{\downarrow i+1}(0, \lambda) \quad (8)$$

$$F_{\uparrow i}(H_i, \lambda) = F_{\uparrow i+1}(0, \lambda) \quad (9)$$

In (6) through (9) the two subscripts on F define the direction (\downarrow , \uparrow) and the layer number (i), and H_i is the layer thickness. The remaining $2N$ equations are obtained by applying the differential equations (1) and (2) at the top of every layer. This is done at the top of the layer, since $z = 0$ simplifies the resulting equations.

Substituting the general solutions (4) and (5) into these $4N$ equations yields a system of $4N$ equations for each wavelength. Once the system is solved and values of A_i , B_i , C_i , and D_i are determined, the upwelling and downwelling irradiance can be calculated anywhere in the medium. For computing irradiances, the depth z is with respect to the layer rather than the entire medium.

Two parameters of particular interest are the spectral

albedo (α_λ) and the transmittance (T_λ). The spectral albedo is the ratio of the reflected and incident irradiance, or

$$\alpha_\lambda = \frac{(R_0 F_0 + D_1)}{F_0}$$

The spectral transmittance is the ratio of the transmitted and the incident irradiance, or

$$T_\lambda = \frac{(A_N \sinh(\kappa_N H_N) + B_N \cosh(\kappa_N H_N))}{F_0}$$

These spectral values can be integrated over wavelength to give bulk values of albedo (α_B)

$$\alpha_B = \frac{\int \alpha_\lambda F_0(\lambda) d\lambda}{\int F_0(\lambda) d\lambda}$$

and transmittance (T_B)

$$T_B = \frac{\int T_\lambda F_0(\lambda) d\lambda}{\int F_0(\lambda) d\lambda}$$

For biological purposes, the spectral downwelling irradiance at the underside of the ice is of considerable interest. Since it is the number of photons of particular wavelengths which controls biological activity, irradiance is presented in terms of photons of wavelength λ per unit area per time, rather than the more familiar units of watts per square meter [Soo Hoo *et al.*, 1987]. The basic unit for this is an einstein (E), which is equal to the energy of a mole of photons of wavelength λ . More precisely, an einstein is defined as

$$E_n = \frac{nhc}{\lambda}$$

where n is Avogadro's number (6.025×10^{23}), h is Planck's constant (6.625×10^{-34} J/s), and c is the speed of light (3×10^{17} nm/s). The total photosynthetically active radiation (PAR) is equal to the irradiance (units of $\mu\text{E}/\text{m}^2\text{s}$) integrated from 400 to 700 nm.

THE SEA ICE MODEL

We now take the general form of the model and adapt it to the specific case of a sea ice cover. The input parameters needed for the model are spectral scattering and extinction coefficients for each medium type considered, layer thickness, and optionally the incident spectral irradiance.

Nine medium types are included in the sea ice model: (1) cold dry snow, (2) melting wet snow, (3) ice colder than the eutectic point, (4) surface scattering layer of white ice, (5) interior portion of white ice, (6) cold blue ice, (7) melting blue ice, (8) bubble free fresh ice, and (9) clear Arctic water. Spectral extinction coefficients for these nine types are plotted in Figure 2. The extinction coefficients for ice types 1, 4, 5, and 7 came directly from Grenfell and Maykut [1977], type 3 values are from Perovich [1979], and type 8 values are from Grenfell and Perovich [1981]. The clear Arctic water (type 9) values were obtained from Grenfell [1979], who

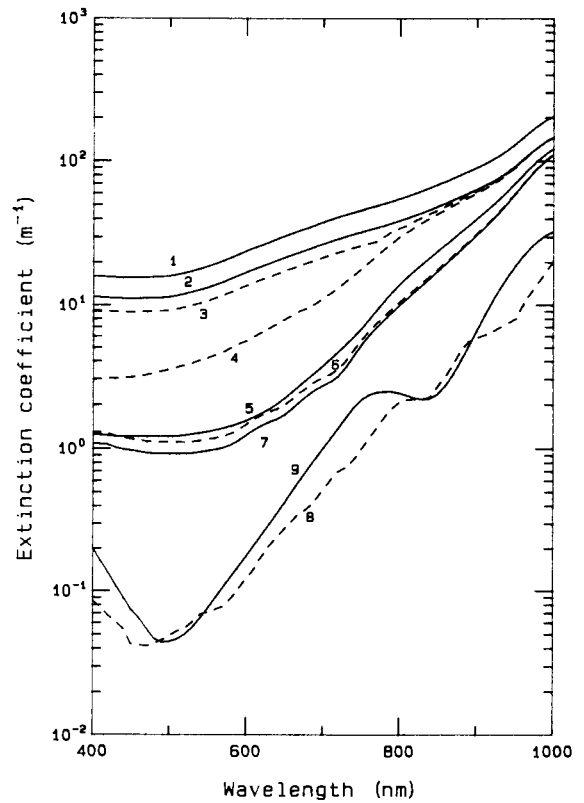


Fig. 2. Spectral extinction coefficients for nine medium types used in the sea ice radiative transfer model: 1, dry snow; 2, ice colder than the eutectic point; 3, melting snow; 4, surface scattering layer of white ice; 5, interior portion of white ice; 6, cold blue ice; 7, melting blue ice; 8, clear Arctic water; and 9, bubble free fresh ice.

applied Gulf Stream measurements made by Tyler and Smith [1970] to the polar oceans. The melting wet snow and cold blue ice values were obtained by adjusting the scattering coefficients for cold dry snow and melting blue ice in order to reproduce spectral albedos reported by Grenfell and Perovich [1984] for melting snow and cold blue ice. Extinction coefficients beyond 800 nm have been extrapolated from observations and are somewhat suspect. Because of experimental errors due to light leakage and to lack of spectral resolution, extinction coefficients at longer wavelengths are quite possibly larger than the values reported here.

Values for the scattering coefficients were not explicitly reported in any of the papers cited above, though spectral albedos were presented. Therefore we determined scattering

TABLE 1. Scattering Coefficients (m^{-1}) for Nine Medium Types

Medium	Scattering Coefficient, m^{-1}
Cold dry snow	800
Melting wet snow	160
Ice below eutectic	160
White ice scattering	120
White ice interior	2.5
Cold blue ice	1.8
Melting blue ice	1.2
Buddle-free ice	0.0
Clear Artic water	0.0

The scattering coefficients are constant with wavelength.

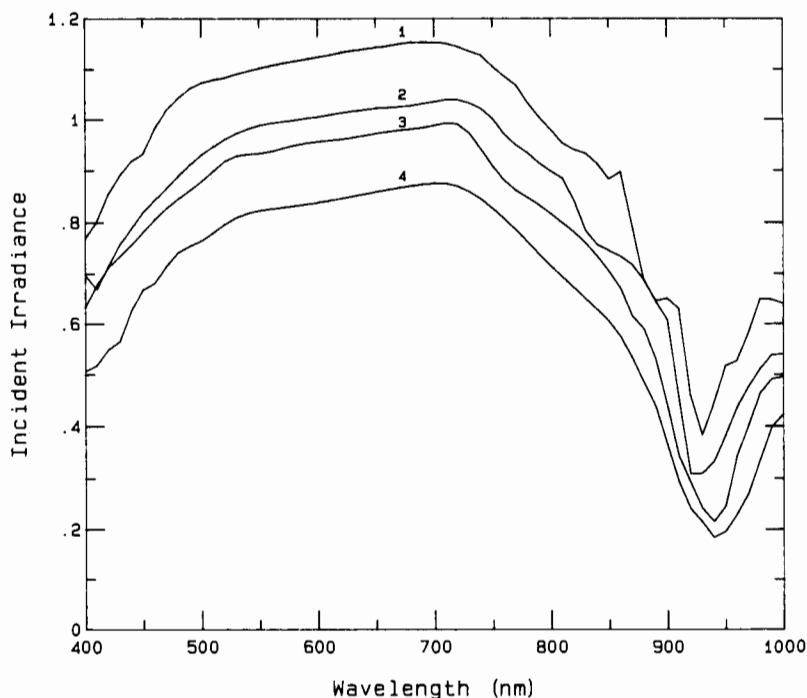


Fig. 3. Normalized values of spectral incident irradiance under Arctic conditions: 1, clear skies; 2, light clouds, solar disk visible; 3, cloudy, solar disk barely visible; and 4, heavy overcast, solar disk not visible [from Grenfell and Perovich, 1984]. These values are multiplied by wavelength-integrated incident irradiance (400–2500 nm) to obtain spectral incident irradiances.

coefficients by inputting the extinction coefficients from Figure 2 into the two-stream model and varying the scattering coefficient to reproduce the reported albedos. In the visible and near-infrared, the scattering inhomogeneities are much larger than the wavelength, and the scattering coefficient does not vary with wavelength [Grenfell, 1983; Bohren and Huffman, 1983]. The bubble free ice and clear Arctic water cases were assumed to be purely absorbing media. Scattering coefficients (Table 1) varied from zero for bubble free fresh ice and Arctic water to 800 m^{-1} for cold dry snow.

Spectral albedos and transmittances do not depend on the spectral composition of the incident radiation, so if these are the parameters of interest, $F_0(\lambda)$ is not needed. However, there are other situations, particularly in biological applications, where absolute values of upwelling or downwelling irradiance are desired. In these cases, $F_0(\lambda)$ must be specified. Representative Arctic spectra of incident solar irradiances measured at Point Barrow, Alaska, were incorporated into the model [Grenfell and Perovich, 1984]. The sky conditions for the four curves presented in Figure 3 were (1) clear skies; (2) light clouds, solar disk clearly visible; (3) cloudy, solar disk barely visible; and (4) heavy overcast, solar disk not visible. The plotted values are normalized and represent the fraction per nanometer of the total incident irradiance and thus must be multiplied by the total incident irradiance from 400 to 2400 nm. One somewhat disturbing feature of the curves is that the maxima are about 700 nm, which is contrary to other observations [Gast, 1960]. It is uncertain whether the maxima are indicative of a reddening of the sun due to low solar angle or are a manifestation of 10% to 15% uncertainties in absolute spectral irradiances (T.C. Grenfell, personal communication, 1988). This illus-

trates a need for additional precise measurements of incident spectral irradiance under Arctic conditions.

Both the albedo and the upwelling irradiance at the surface can have a specular reflection component (R_0). This is strictly a surface phenomenon arising from index of refraction differences at the interface between two media. The indices of refraction of ice and water are so close, 1.31 and 1.33 respectively, that R_0 at the bottom ice-water boundary is assumed to be zero. However since air has an index of refraction of 1, R_0 at the surface is not negligible. Under diffuse sky conditions, R_0 for air-ice or air-water will be 0.05 [Perovich and Grenfell, 1982]. The dry and wet snow types have a rough granular surface, and we cannot distinguish specular reflection from scattering, so we assume $R_0 = 0.0$.

A computer program utilizing the solution presented in the theory section was written to calculate the upwelling and downwelling irradiances and associated parameters for an arbitrary medium consisting of up to 15 distinct layers. The model allows selection of the number, type, and thickness of layers, along with the incident shortwave irradiance, sky conditions and spectral range of interest. Output parameters include spectral values of surface upwelling irradiance, bottom downwelling irradiance, albedo, transmittance, and PAR and wavelength-integrated values of bulk albedo, transmittance, transmitted flux, and PAR. Because of the relative simplicity of the model, solutions can be quickly calculated on a personal computer.

APPLICATIONS OF THE MODEL

We shall demonstrate the utility of the radiative transfer model by applying it to three distinct cases: (1) obtaining a

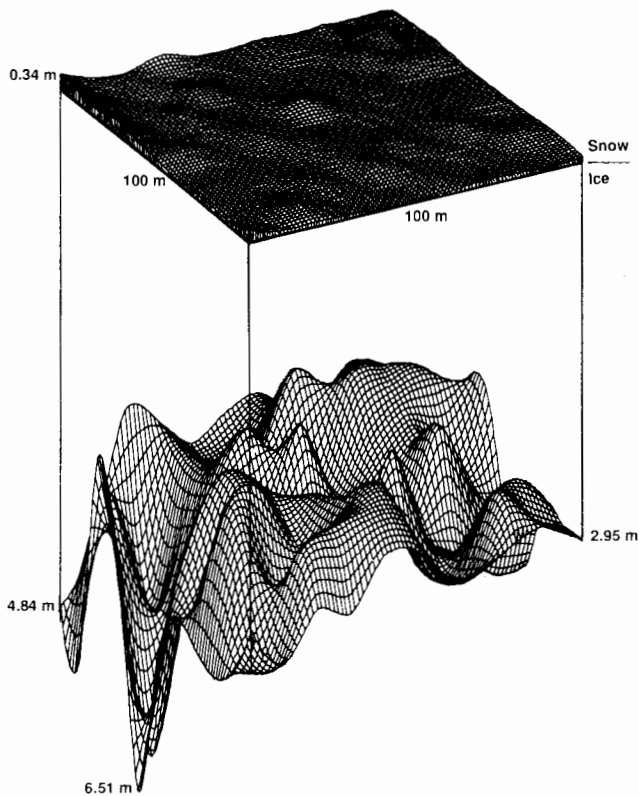


Fig. 4. Snow and ice thickness data from W. B. Tucker (personal communication, 1988). The bottom and top surfaces represent the thicknesses of the ice and the snow cover, respectively. The thickness data were taken at 10-m spacings on a 100 by 100 m grid.

two-dimensional spatial picture of the transmitted radiation field through a cold ice cover which varies in X and Y , (2) monitoring temporal changes in light transmission through melting ice, and (3) determining combined spectral and temporal variations in light transmission. The major focus of these three examples will be on the transmitted spectral radiation, with some attention paid to spectral albedos. In addition to showing the capabilities of the model, the examples have been selected to illustrate the effects of variations in ice thickness, snow cover, surface conditions, and ice types on the optical properties.

Spatial Variations

W. B. Tucker (personal communication, 1988) used a hot water drill to perform a detailed mapping of ice and snow thickness on several floes in the Beaufort Sea. Figure 4 summarizes the snow and ice thickness data from one of these floes, where 121 ice thicknesses were measured for a 100 by 100 m section using a 10-m grid. This area consisted of deformed multiyear ice with a primarily columnar crystal texture. The observations were made in April, so the snow cover was cold and dry and the ice was cold but not below the eutectic point. Ice thicknesses ranged from 1.8 to 6.5 m with a mean of 3.01 m, while snow thicknesses varied from 0 to 0.34 m with a mean of 0.07 m.

The ice cover is assumed to be relatively homogeneous, consisting of interior white ice. Thus variations in light transmission are due primarily to differences in snow and ice thickness. The two-dimensional spatial distribution of transmitted light at 470 nm is plotted in Figure 5. The fraction

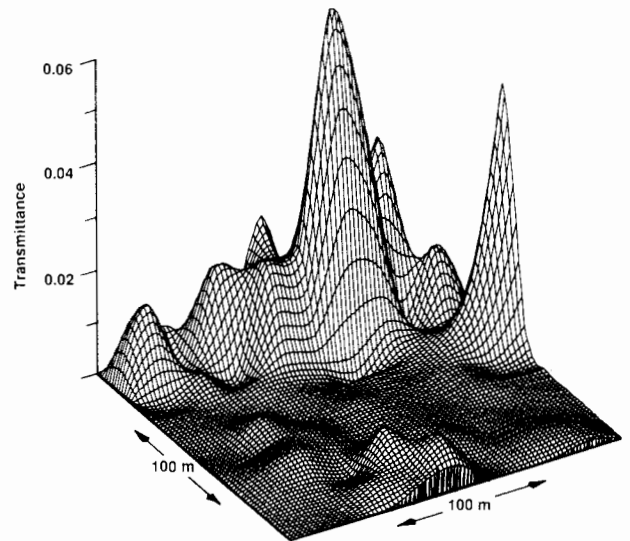


Fig. 5. Spatial distribution of light transmittance at 470 nm for ice and snow conditions of Figure 4.

transmitted spans over 5 orders of magnitude from 0.88×10^{-6} to 0.63×10^{-1} . Features in this plot do not necessarily correlate with the ice thickness topography. The peaks in transmitted light correspond to areas of bare ice, while minimum values occur where the snow was the deepest. Distributions at other wavelengths are similar in shape to Figure 5 but have reduced magnitudes.

The question arises whether this detailed spatial computation results in a better representation of light reflection and transmission for this area. To address this issue, spectral albedos and transmittances were calculated for the 121 points on Tucker's thickness grid. These values were then averaged to generate an areal estimate for the region and are plotted as curve 1 in Figure 6. For comparison, another areal estimate was computed more simplistically by first determining the mean snow and ice thickness and then calculating spectral values for this single case (curve 2). As curves 1 and 2 indicate, there is a significant disparity between these two

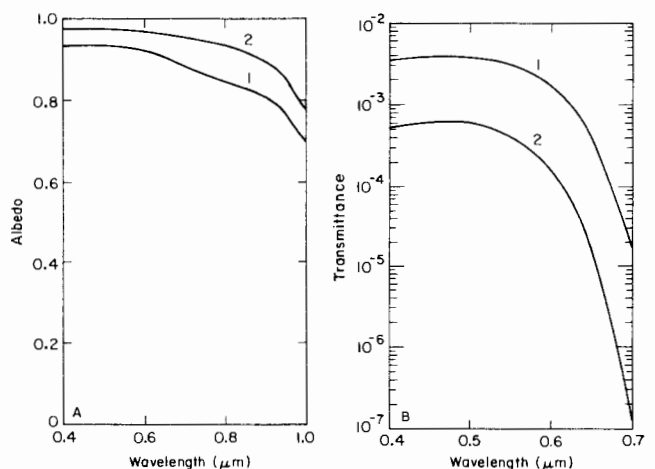


Fig. 6. Areal averaged values of spectral albedo and transmittance for ice cover of Figure 5. Curve 1 is the average of the albedos and transmittances computed for the 121 grid points. In curve 2 the average snow and ice thicknesses of the grid were determined, then used to calculate the spectral albedos and transmittances.

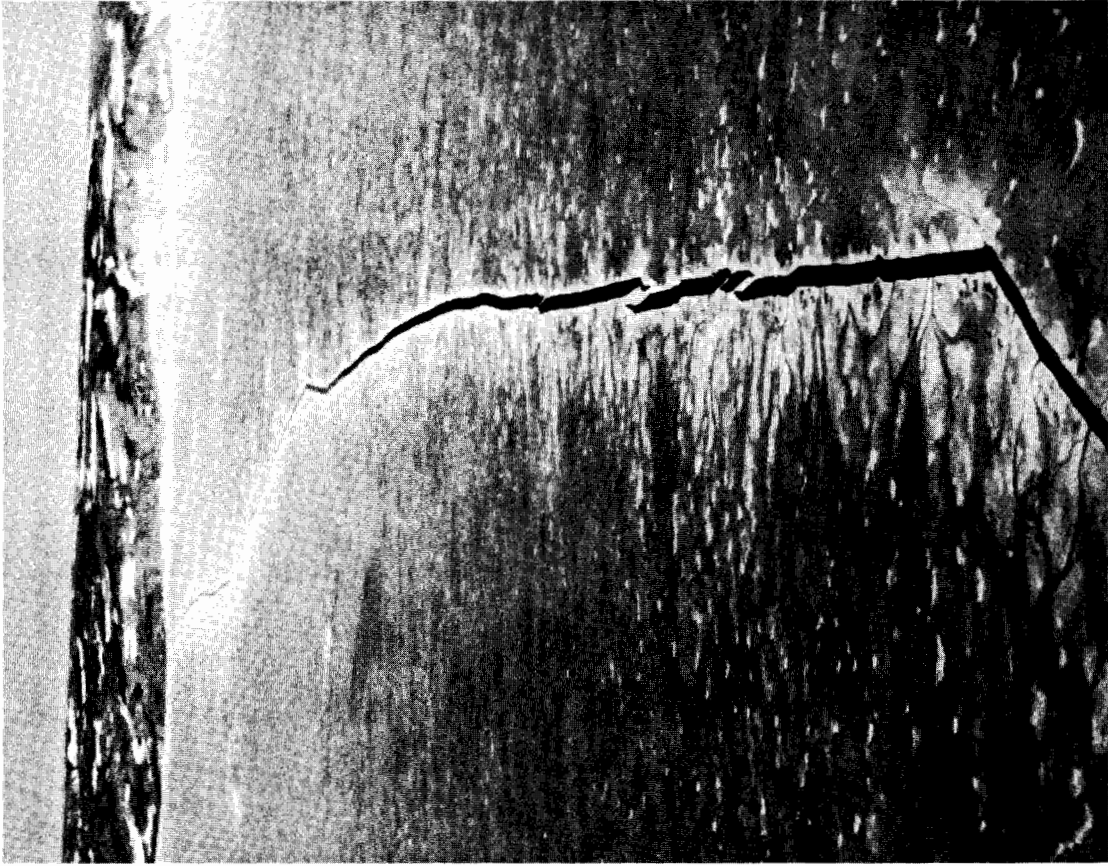


Fig. 7b

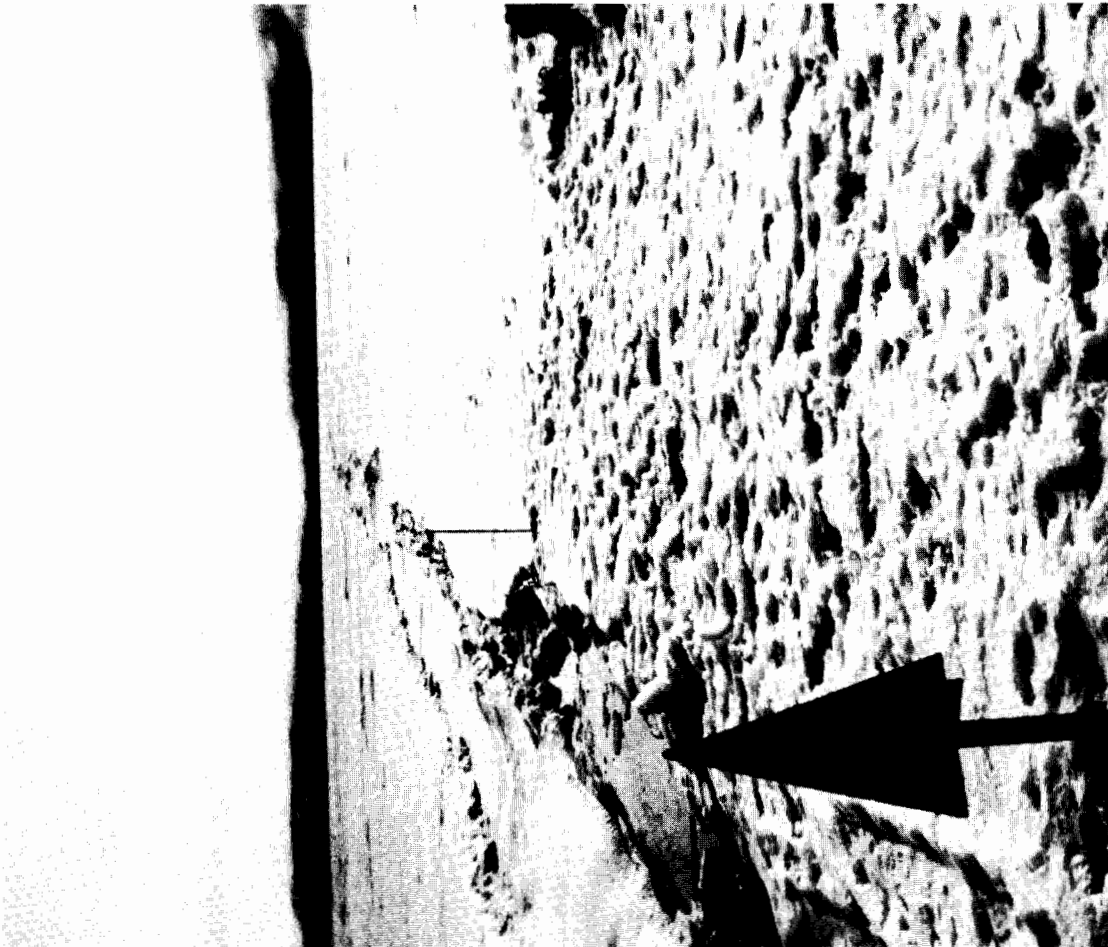


Fig. 7a

Fig. 7. Photographs illustrating surface conditions on Mould Bay ice cover; melting snow on June 21 and heavily ponded ice on July 2.

TABLE 2. Environmental Conditions for Mould Bay Ice Cover

Date, 1982	Ice Thickness, m	Surface Conditions, m	Incident Shortwave, W/m ²	Cloud Conditions
June 20	2.22	0.30 DS	310	heavy overcast, solar disk not visible
June 21	2.22	0.30 MS	316	light clouds, solar disk clearly visible
June 22	2.22	0.20 MS	357	clear skies
June 23	2.22	0.10 MS	352	clear skies
June 24	2.22	0.10 MP	209	heavy overcast, solar disk not visible
June 25	2.20	0.20 MP	199	heavy overcast, solar disk not visible
June 26	2.18	0.10 MP	178	heavy overcast, solar disk not visible
June 27	2.16	0.05 MP	353	light clouds, solar disk clearly visible
June 28	2.14	0.05 MP	235	cloudy, solar disk barely visible
June 29	2.12	0.05 MP	332	clear skies
June 30	2.10	0.10 MP	326	clear skies
July 1	2.03	0.05 MP	231	cloudy, solar disk barely visible
July 2	1.96	0.10 MP	337	clear skies
July 3	1.89	0.05 MP	228	cloudy, solar disk barely visible
July 4	1.83	0.05 MP	126	heavy overcast, solar disk not visible
July 5	1.76	0.05 MP	170	heavy overcast, solar disk not visible
July 6	1.69	0.05 MP	241	cloudy, solar disk barely visible
July 7	1.62	0.05 MP	313	light clouds, solar disk clearly visible
July 8	1.56	0.05 MP	335	clear skies
July 9	1.53	0.05 MP	312	clear skies
July 10	1.49	0.05 MP	312	clear skies

The surface conditions give the thickness and type of surface layer, where DS is dry snow, MS is melting snow, and MP is melt pond.

methods, with the simplistic method yielding albedos roughly 0.05 higher and transmittances nearly an order of magnitude lower than the more detailed analysis. Of course this is not surprising, since radiative transfer processes are more exponential than linear with depth. As a direct consequence of this the actual areal-averaged transmittance will always be greater than or equal to values computed by using mean snow and ice thicknesses for the area. The difference is particularly pronounced for cases such as this in which part of the area is snow free.

Temporal Variations

Even a spatially uniform ice sheet can be optically complex when it is undergoing temporal changes. From an optical perspective the most dramatic changes occur in the early portion of the melt season as the ice evolves from an opaque, snow-covered medium to translucent bare or ponded ice. This transition is of particular interest biologically, since some of the organisms living in and under the ice are light limited and the removal of the snow cover governs the onset of biological activity. To illustrate this point, we will examine the optical evolution of a topographically simple ice sheet during the early melt season. In the spring of 1982, Mould Bay fiord (Prince Patrick Island in the Canadian archipelago) was covered by 2.2 m of flat, undeformed, first-year ice overlain by 0.30 m of snow [Perovich, 1983]. The snow melted quickly between June 21 and 25, transforming the entire ice sheet into a melt pond for a few days until it isostatically readjusted, leaving predominantly melting blue ice and shallow melt ponds with some patches of drained white ice. These changes in surface conditions are illustrated in the photographs in Figure 7. By July 10 the ice had thinned to 1.46 m with most of the melting occurring during July. Table 2 summarizes ice thickness, snow depth, pond depth, incident shortwave irradiance, and cloud cover

for June 20 to July 10, 1982. With these data as input the radiative transfer model was run for each day.

In Figure 8, albedo is plotted as a function of wavelength and time. The first decrease in albedo occurred on June 21 when the snow began to melt. This drop was somewhat greater at longer wavelengths. There was a precipitous drop 3 days later, when the snow melted and the surface became completely covered by melt ponds. After this point spectral albedos were fairly constant with some small variations due to changes in pond depths.

Spectral values of transmitted PAR for the same time period are plotted in Figure 9. The snow cover was still present for the first few days and an insignificant amount of light was transmitted. Once the snow melted and ponds formed, PAR values increased sharply, especially at shorter wavelengths. As the ice thinned over the next 2 weeks there was a general upward trend in transmitted PAR. This upward trend increased in July as the ice thinning accelerated. The occasional decrease, such as the July 4 decline, occurred on cloudy days with low incident solar irradiance. The spectral peak of transmitted PAR was at 530 nm. Total PAR displayed a similar behavior, with an increase of more than an order of magnitude as the snow cover began to melt (June 20–21), then a sharp increase of a factor of 100 as the snow completely melted and the ice surface became flooded (June 21–24), and finally a gradual tenfold increase as melting progressed and the ice cover thinned (June 25 to July 10).

Spatial and Temporal Variations

In the more dynamically active regions of the Arctic, simple undeformed ice sheets, as found in Mould Bay, are quite scarce. More common is an ice cover with some surface topography, perhaps a ridge, a few hummocks, a low area or two, and typically a variable snow cover. In such a

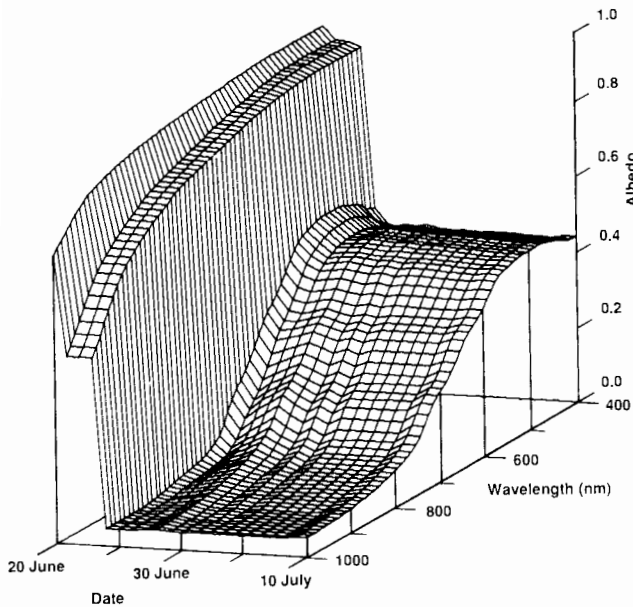


Fig. 8. Temporal evolution of spectral albedo for the Mould Bay ice cover.

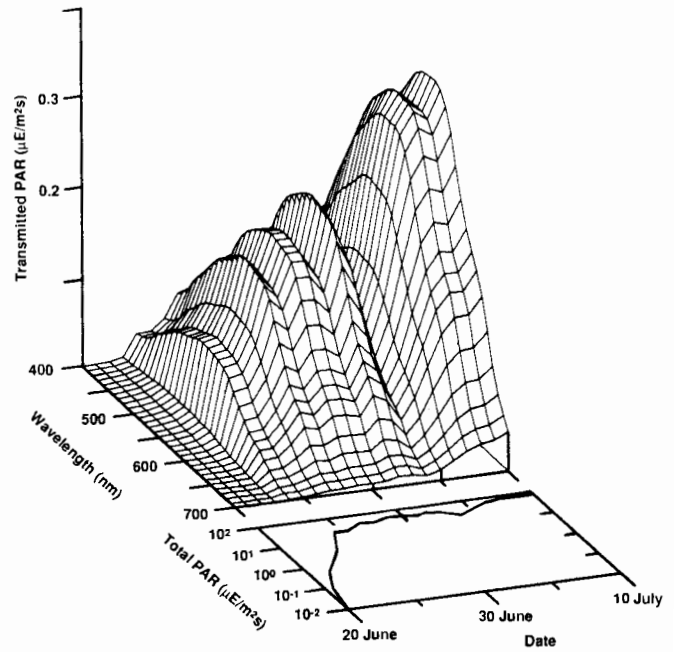


Fig. 9. Temporal evolution of spectral and total PAR for the Mould Bay ice cover. Units of PAR are $\mu\text{E}/\text{m}^2\text{s}$.

case, spatial variations in ice conditions can further complicate the temporal evolution of the transmitted radiation field.

To illustrate the combined effects of spatial and temporal variations, let us examine three sites that were monitored from June 20 to July 7 during the 1984 Marginal Ice Zone Experiment [Maykut and Perovich, 1985]. These sites were all within 5 m of one another along a small pressure ridge. Site 1 was on the side of the ridge where the snow cover was deepest and had snow present through July 7. Site 2 was at the top of the ridge, where the surface was snow free, though covered with 0.03 m of melting granular white ice throughout the experiment. Site 3 was initially covered by 0.21 m of snow, which melted by July 3. A melt pond formed at this

site, reaching a depth of 0.20 m by July 7. Snow and ice thicknesses, surface conditions, and the incident radiation field for these three sites are summarized in Table 3.

Spectral albedos for the three sites are summarized in Figure 10. Surface conditions at site 2 (dashed line) remained constant during the experiment and this was reflected in an albedo that was temporally invariant. Site 1 (shaded envelope) exhibited a very slight decrease in time due to the thinning of the snow cover. Changes in spectral albedo were most dramatic at site 3, where surface conditions evolved from cold dry snow to melting snow to bare white ice to

TABLE 3. Environmental Conditions for MIZEX 84 Sites

Date, 1984	Cloud Conditions	Incident Shortwave, W/m^2	Snow (H_s) and ice (H_i) thickness, m					
			Site 1		Site 2		Site 3	
			H_s	H_i	H_s	H_i	H_s	H_i
June 20	Clear skies	300	0.38	2.02	0.00	3.87	0.21	3.32
June 21	Clear skies	305	0.34	2.01	0.00	3.83	0.18	3.29
June 22	Light clouds, solar disk visible	215	0.32	2.01	0.00	3.82	0.16	3.28
June 23	Light clouds, solar disk visible	220	0.29	2.00	0.00	3.79	0.15	3.27
June 24	Clear skies	277	0.28	1.98	0.00	3.79	0.14	3.26
June 25	Cloudy, solar disk barely visible	183	0.27	1.96	0.00	3.78	0.14	3.25
June 26	Cloudy, solar disk barely visible	194	0.25	1.92	0.00	3.76	0.11	3.25
June 27	Cloudy, solar disk barely visible	172	0.24	1.85	0.00	3.74	0.11	3.22
June 28	Cloudy, solar disk barely visible	171	0.24	1.83	0.00	3.73	0.10	3.20
June 29	Cloudy, solar disk barely visible	159	0.23	1.79	0.00	3.69	0.06	3.16
June 30	Cloudy, solar disk barely visible	168	0.19	1.76	0.00	3.65	0.03	3.13
July 1	Heavy overcast, solar disk not visible	114	0.17	1.71	0.00	3.60	0.02	3.11
July 2	Cloudy, solar disk barely visible	170	0.16	1.68	0.00	3.59	0.01	3.10
July 3	Cloudy, solar disk barely visible	157	0.15	1.67	0.00	3.57	0.00	3.06*
July 4	Heavy overcast, solar disk not visible	136	0.13	1.65	0.00	3.54	0.00	3.00
July 5	Heavy overcast, solar disk not visible	137	0.11	1.62	0.00	3.49	0.00	2.91
July 6	Heavy overcast, solar disk not visible	104	0.10	1.60	0.00	3.40	0.00	2.78
July 7	Heavy overcast, solar disk not visible	100	0.04	1.60	0.00	3.23	0.00	2.64

The incident shortwave irradiance is the mean daily value.

*H for site 3 designates the formation of a melt pond.

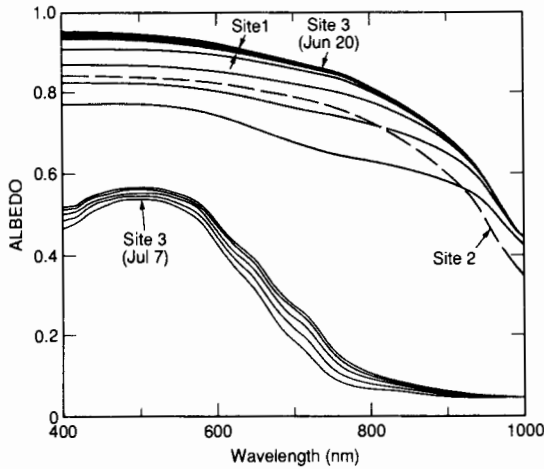


Fig. 10. Spectral albedos from sites 1, 2, and 3. The shaded area represents albedos for site 1, the dashed line shows the albedo at Site 2, and the series of curves depicts daily albedos at site 3 from June 20 (high) to July 7 (low). Note that the June 20 curve for site 3 is coincident with the maximum site 1 albedo.

melting blue ice to a melt pond with a corresponding continual decrease in albedo. Daily albedos at site 3 from June 20 to July 7 are represented by the family of curves in Figure 10.

Transmitted values of total PAR for the three sites are presented in Figure 11. Total transmitted PAR integrated over the 18-day period was $17.6 \mu\text{E}/\text{m}^2\text{s}$ for site 1, 12.6 for site 2, and 31.6 for site 3. Values at sites 1 and 3 were small initially, but increased as the snow cover melted. Transmitted PAR was the greatest at site 3 after the snow melted and a melt pond formed. At site 2, results were fairly constant during the entire observation period. There was a sharp increase in total transmitted PAR at site 1 between July 6 and 7 as the snow thickness decreased from 0.10 to 0.04 m. On June 20, site 2 had the highest transmission, yet by the end of the experiment it was the lowest. In fact, readings at site 3 increased from 20% of site 2 PAR to 500% of site 2 PAR. Even over this small 5-m spatial scale, at a particular time, differences in transmitted PAR between the three sites were as large as a factor of 5, illustrating the potential inaccuracies

of estimating transmitted PAR from a single set of measurements.

Transmitted PAR as a function of time and wavelength for sites 1, 2, and 3 is plotted in Figure 12. The contours are isopleths of the base 10 logarithm of transmitted PAR (0.2 intervals). The sharp dropoff of PAR at wavelengths beyond 650 nm is evident in all three cases. Maximum PAR is transmitted between 450 and 550 nm. Temporal changes were greatest at site 3, with an increase in PAR at 470 nm of one and a half orders of magnitude. In essence, the formation of the melt pond at site 3 is analogous to opening a window in the ice cover.

DISCUSSION

A sea ice cover can have tremendous variability in the reflected and transmitted radiation fields. Ice thickness can vary from centimeter-thick nilas to ridges tens of meters thick, while snow depths can range from zero to a meter or more. Over horizontal distances of a few meters, surface conditions can change from snow-covered ice to bare white ice to ponded ice. As we have seen in the three case studies presented herein, this can result in variations in light transmittance of several orders of magnitude. Temporal evolution during the melt cycle is also quite significant. Removal of the snow cover results in a reduction in albedo and a sharp increase in transmittance. The formation of melt ponds causes a further decrease in albedo and enhancement of transmittance.

This complexity makes estimation of areally or temporally averaged values of reflected or transmitted light difficult. However, such values are important for a number of applications, including assessments of biological activity, internal ice melting, and regional albedos. Single point measurements of albedo or transmittance are inadequate to define areal averages, while detailed measurements on a large spatial scale are not practical.

The model presented in this paper provides a mechanism for estimating light reflection and transmission for such complex ice covers. Because of the model's computational simplicity the optical properties of an ice cover can be represented in spatial or temporal detail. The input param-

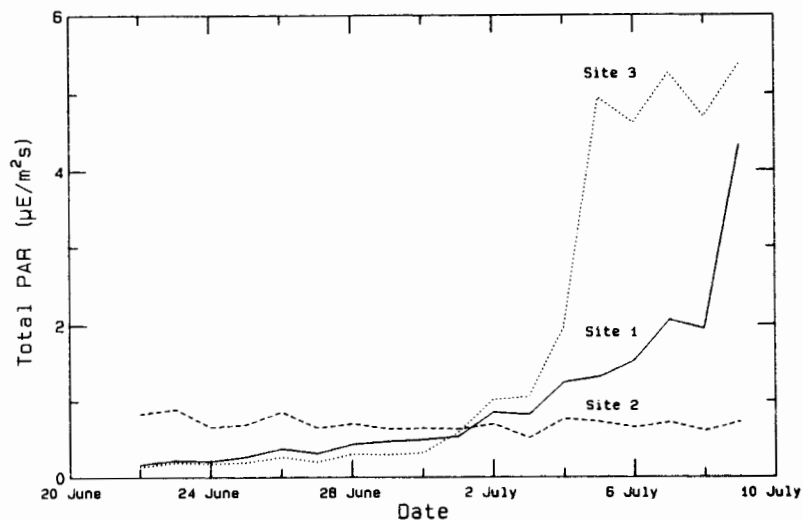


Fig. 11. Total PAR ($\mu\text{E}/\text{m}^2\text{s}$) as a function of time for sites 1, 2, and 3.

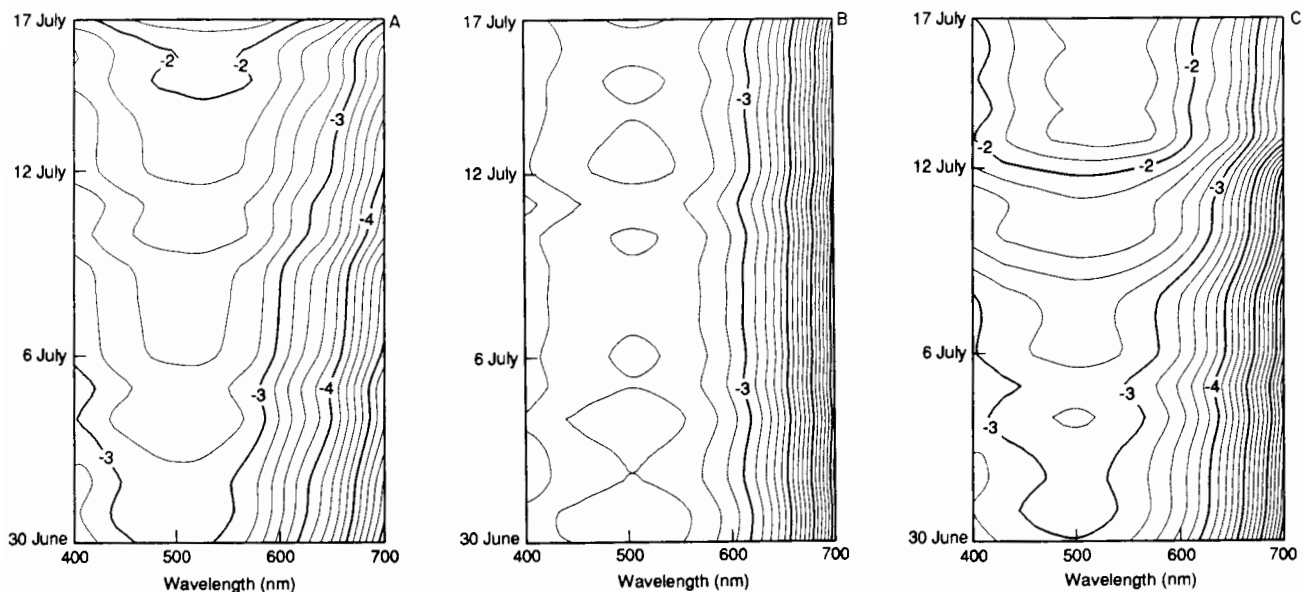


Fig. 12. Contours of spectral PAR for (a) site 1, (b) site 2, and (c) site 3. The contours represent orders of magnitude of spectral transmitted PAR ($\mu\text{E}/\text{m}^2\text{s}$), for example the -2 contour denotes a PAR of 10^{-2} ($\mu\text{E}/\text{m}^2\text{s}$). The contour interval is 0.2.

ters needed for the computation are all easily observable quantities: ice thickness, snow depth, ice surface conditions, and a qualitative description of the medium's composition in terms of ice and snow types. Once the structural description is specified, spectral albedos, PAR values, and transmittances can be calculated.

This method works well for small areas with an observer present, but is it applicable for large-scale regional estimates? Drilling thickness holes at 10-m intervals over the entire Arctic basin is neither appealing nor practical. Ideally, we would generate regional estimates by using remote sensing to obtain the model input parameters. While present-day remote sensing sources cannot provide a complete description of the snow cover and the thickness and internal structure of the ice, they can provide data on surface conditions. This information, taken in conjunction with some simple assumptions, can furnish useful input to the model. The two most important factors for regional estimates of albedo and transmittance are the area of open water and the area of snow-covered ice, both of which can be determined from remote sensing data. Light transmission through the open water can be computed using the Arctic water case, and we can assume that any snow-covered ice is optically thick with negligible transmission. For the area covered by bare ice, satellite imagery can be used to determine the relative amounts of white ice and ponded ice. Though ice thicknesses cannot be observed directly from space, they can be approximated from thickness distributions derived from other sources such as submarine upward-looking sonar profiles. In this fashion we can calculate at least a rough regional estimate of the reflected and transmitted light.

Currently, the model is limited to nine snow and ice types. While these types constitute a considerable collection, there are a few significant omissions. For example, there is a scarcity of data on the optical properties of Antarctic pack ice. Because of the significant biological activity within and beneath the Antarctic ice cover, this is a region of extreme

interest for optical modeling. Structurally, Antarctic sea ice is quite different from Arctic ice [Gow *et al.*, 1982], with large expanses of pancake ice and a preponderance of frazil rather than columnar crystals. This difference in ice structure presumably results in some disparity in optical properties. The presence of contaminants in the ice, such as organisms, would also change its optical properties. Measurements are needed to determine spectral scattering and extinction coefficients for these ice types to extend the model to include these cases. A knowledge of the optical characteristics of various organisms would be particularly useful, allowing the effects of biological activity on the reflected and transmitted radiation field to be investigated. In addition, complex biological communities with different organisms at different levels within and under the ice could be investigated.

Acknowledgments. The author would like to thank Kathleen Jones for her mathematical expertise and T. C. Grenfell for the many helpful discussions. Funding for this work was provided by DA project 4A161102AT24 and ONR contract N0001488WM24013.

REFERENCES

- Bohren, C. F., and D. R. Huffman, *Absorption and Scattering of Light by Small Particles*, 530 pp., John Wiley, New York, 1983.
- Buckley, R. G., and H. J. Trodahl, Thermally driven changes in the optical properties of sea ice, *Cold Reg. Sci. Technol.*, 14, 201-204, 1987.
- Chandrasekhar, S. C., *Radiative Transfer*, 393 pp., Dover, New York, 1960.
- Dunkle, R. V., and J. T. Bevens, An approximate analysis of the solar reflectance and transmittance of a snow cover, *J. Meteorol.*, 13, 212-216, 1956.
- Gast, P. R., Solar radiation, in *Handbook of Geophysics*, edited by C. F. Campan *et al.*, Macmillan, New York, 1960.
- Gow, A. J., S. F. Ackley, W. F. Weeks, and J. W. Govoni, Physical and structural characteristics of Antarctic sea ice, *Ann. Glaciol.*, 3, 113-117, 1982.
- Grenfell, T. C., The effects of ice thickness on the exchange of solar radiation over the polar oceans, *J. Glaciol.*, 22, 305-320, 1979.

- Grenfell, T. C., A theoretical model of the optical properties of sea ice in the visible and near infrared, *J. Geophys. Res.*, **88**, 9723-9735, 1983.
- Grenfell, T. C., and G. A. Maykut, The optical properties of ice and snow in the Arctic Basin, *J. Glaciol.*, **18**, 445-463, 1977.
- Grenfell, T. C., and D. K. Perovich, Radiation absorption coefficients of polycrystalline ice from 400-1400 nm, *J. Geophys. Res.*, **86**, 7447-7450, 1981.
- Grenfell, T. C., and D. K. Perovich, Spectral albedos of sea ice and incident solar irradiance in the southern Beaufort Sea, *J. Geophys. Res.*, **89**, 3573-3580, 1984.
- Maykut, G. A., and D. K. Perovich, MIZEX 84 Heat and Mass Balance Data, *Rep. APL-UW 12-85*, 73 pp., Appl. Phys. Lab., Univ. of Wash., Seattle, 1985.
- Maykut, G. A., and D. K. Perovich, The role of shortwave radiation in the summer decay of a sea ice cover, *J. Geophys. Res.*, **92**, 7032-7044, 1987.
- Maykut, G. A., and N. U. Untersteiner, Some results from a time dependent, thermodynamic model of sea ice, *J. Geophys. Res.*, **76**, 1550-1575, 1971.
- Perovich, D. K., The optical properties of young sea ice, M.S. thesis, 151 pp., Univ. of Wash., Seattle, 1979.
- Perovich, D. K., On the summer decay of a sea ice cover, Ph.D. dissertation, 176 pp., Univ. of Wash., Seattle, 1983.
- Perovich, D. K., A two-stream, multilayer spectral radiative transfer model, *CRREL Rep. 89-XX*, 17 pp., U.S. Army Cold. Reg. Res. and Eng. Lab., Hanover, N. H., 1989.
- Perovich, D. K., and T. C. Grenfell, Laboratory studies of the optical properties of young sea ice, *J. Glaciol.*, **27**, 331-346, 1981.
- Perovich, D. K., and T. C. Grenfell, A theoretical model of radiative transfer in young sea ice, *J. Glaciol.*, **28**, 341-356, 1982.
- Perovich, D. K., G. A. Maykut, and T. C. Grenfell, Optical properties of ice and snow in the polar oceans, I, Observations, Society of Photo-Optical Instrumentation Engineers Technical Symposium Southeast on Optical and Optoelectronic Systems, 31 March-2 April 1986, Orlando, Florida, *Proc. Soc. Photo Opt. Instrum. Eng.*, **637**, 232-244, 1986.
- Schuster, A., Radiation through a foggy atmosphere, *Astrophys. J.*, **21**, 1-22, 1905.
- SooHoo, T. B., A. C. Palmisano, S. T. Kottmeier, M. P. Lizotte, S. L. SooHoo, and C. W. Sullivan, Spectral light absorption and quantum yield of photosynthesis in sea ice microalgae and a bloom of *Phaeocystis pouchettii* from McMurdo Sound, Antarctica, *Mar. Ecol.*, **33**, 175-189, 1987.
- Trodahl, H. J., R. J. Buckley, and S. Brown, Diffusive transport of light in sea ice, *Appl. Opt.*, **26**, 3005-3011, 1987.
- Tyler, J. E., and R. C. Smith, *Measurements of Spectral Radiance Underwater*, 103 pp., Gordon and Breach, New York, 1970.
- Warren, S. G., Optical properties of snow, *Rev. Geophys.*, **20**, 67-89, 1982.
-
- D. K. Perovich, Snow and Ice Branch, U.S. Army Cold Regions Research and Engineering Laboratory, 72 Lyme Road, Hanover, NH 03755.

(Received July 21, 1989;
accepted October 2, 1989.)